Spatial-nonlocality-induced non-Markovian electromagnetically induced transparency in a single giant atom

Y. T. Zhu [1,2,3] S. Xue [1,2,3,*] R. B. Wu,[4] W. L. Li,[4] Z. H. Peng,[5] and M. Jiang [6]

[1]*Department of Automation, Shanghai Jiao Tong University, Shanghai 200240, People's Republic of China*
[2]*Key Laboratory of System Control and Information Processing, Ministry of Education of China, Shanghai 200240,*
People's Republic of China
[3]*Shanghai Engineering Research Center of Intelligent Control and Management, Shanghai 200240, People's Republic of China*
[4]*Center for Intelligent and Networked Systems, Department of Automation, Tsinghua University, Beijing 100084, People's Republic of China*
[5]*Key Laboratory of Low-Dimensional Quantum Structures and Quantum Control of Ministry of Education, Key Laboratory for Matter*
Microstructure and Function of Hunan Province, Department of Physics and Synergetic Innovation Center for Quantum Effects
and Applications, Hunan Normal University, Changsha 410081, People's Republic of China
[6]*School of Electronics and Information Engineering, Soochow University, Suzhou 215006, People's Republic of China*

The nonlocal waveguide coupling of giant atoms can bring up novel physics and applications. In this paper, we find unconventional electromagnetically induced transparency in giant atoms that has not been reported so far. We present a consistent theory for describing the unconventional EIT which includes a real-space scattering method and a time-delayed master equation. Our analysis shows this phenomenon is a full quantum effect led by a quantized interaction between the atom and the waveguide. Our theory shows that it can be observed when the time delay between two neighboring coupling points is comparable to the relaxation time of the atom. This phenomenon results from the inherent nonlocality of the giant atom, which physically forces propagating fields to be standing waves in space and the atom exhibiting retardations in time.

I. INTRODUCTION

Light-matter interaction at the single-photon level lies in the core of modern quantum optics, which has been well investigated in waveguide quantum electrodynamics (waveguide-QED) systems [1,2]. In these systems, artificial atoms based on Josephson junctions strongly couple to a one-dimensional waveguide, which results in a low leakage of photons into the uncontrollable degree of freedom of environments [1–3]. The main advantages of these on-chip structures are their scalability, integration, and tunability of parameters, which makes waveguide-QED systems an excellent platform to study fundamental quantum phenomena and one of the most possible proposals to realize quantum computing [4].

In waveguide-QED systems, artificial atoms are commonly treated as pointlike dipoles as their sizes are much smaller than the wavelength of interacting fields [5,6]. However, recent progress [5,7–22] shows that such treatment is not valid for the so-called artificial atoms who are coupled piezoelectrically to acoustics or capacitively to microwaves at several distant points. In these cases, the effective size of the atoms can be comparable to the wavelength of interacting fields such that the propagating time of the field between the coupling points can no longer be neglected [5,6,23]. Therefore, these artificial atoms are

giant. In giant atoms, effective atom-waveguide couplings are nonlocal due to the interferences among points, which leads to some unconventional phenomena, such as atomic-frequency-dependent Lamb shifts and decay rates [5,7], decoherence-free interactions among several giant atoms with different arrangements [8,18], nonexponential decays [12,16], and single-photon-induced persistent oscillating bound states [17]. Notably, the latter two phenomena are non-Markovian effects.

The above works have revealed some special features of two-level giant atoms, however, a full description of three-level giant atoms is absent. For example, standard electromagnetically induced transparency (EIT) [3,24–29] has been observed in a ladder-type giant atom with either acoustic couplings [30] or microwave couplings [31], but the frequency-dependent properties and non-Markovian effects induced by the nonlocal couplings are still not well understood. This leads to obvious discrepancies between the experimental data and the fit calculated by a master equation without quantized atom-waveguide interactions [31]. Motivated by the above results, we study the EIT phenomena in a single Δ-type giant atom. We first utilize a real-space scattering method [32,33] to characterize the nonlocal properties in space that behave as multipeak scattering spectra. Specifically, we find that the fields inside the outermost coupling points form standing waves via interference between bidirectional propagating modes. Besides, the undesired spontaneous emission can be eliminated rather than suppressed by engineering the multiple-point-coupling structure, which
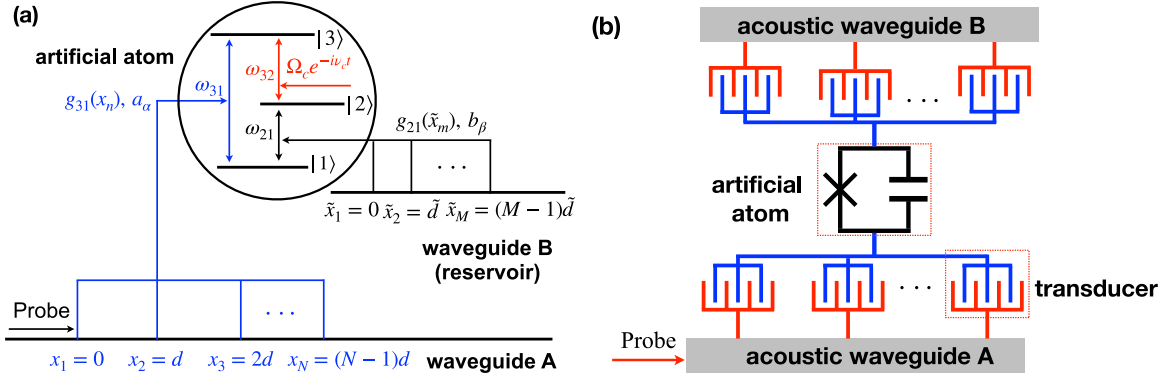
---

*shbxue@sjtu.edu.cn

FIG. 1. (a) Schematic of a Δ-type giant atom. The transition $|1\rangle \leftrightarrow |3(2)\rangle$ is coupled to the waveguide A (B) via multiple coupling points with an equal distance $d(\tilde{d})$. $g_{31}(x_n)$ and $g_{21}(\tilde{x}_m)$ denote the position-dependent coupling strength. Here the waveguide B is taken as a reservoir resulting in the undesired spontaneous emission of the atom, while we take the waveguide A as a channel for a probe field. A classical driving with an angular frequency ν_c and a Rabi frequency Ω_c is applied to the transition $|2\rangle \leftrightarrow |3\rangle$ to induce EIT. (b) Schematic of a possible realization in experiments. An artificial atom couples to two acoustic waveguides through multiple transducers which can convert phonon modes (red lines) to photon modes (blue lines) via the piezoelectric effect, and each transducer serves as an individual coupling point.

turns the Δ-type configuration into a Λ-type artificial atom. This provides a possibility to engineer atomic level structures in future quantum devices. We then present a time-delayed master equation to analyze the nonlocal properties in time which behave as non-Markovian retardations. These two consistent methods solve the abovementioned discrepancies in the existing work [31], which provides a more exact theory on giant atoms.

The remainder of this paper is organized as follows: In Sec. II we provide a theoretical model and equations of motion of a Δ-type giant atom utilizing a real-space scattering method. The unconventional EIT resulting from multiple-point couplings is shown in Sec. III, and we provide a standing-wave explanation in Sec. IV. In Sec. V we propose a time-delayed master equation to describe the non-Markovian effects in the giant atom. Further discussions on the master equation are shown in Sec. VI, including a comparison to the master equation without considering quantized atom-waveguide interactions in Sec. VI A and the validity of Markovian approximation in Sec. VI B. In Sec. VII we conclude this work.

II. MODEL AND EQUATIONS OF MOTION IN REAL-SPACE SCATTERING METHOD

Consider a Δ-type giant atom, whose level structure is shown in the circle of Fig. 1(a). The three energy levels are denoted by $|1\rangle$, $|2\rangle$, and $|3\rangle$ with corresponding transition frequencies ω_{21}, ω_{31}, and ω_{32}, respectively. Here the energy of the ground state $|1\rangle$ is assumed to be zero as a reference. The transitions $|3\rangle \leftrightarrow |1\rangle$ and $|2\rangle \leftrightarrow |1\rangle$ are respectively side coupled to waveguides A and B at multiple points x_n and $\tilde{x}_m$ with indices $n = 1, 2, \ldots, N$, $m = 1, 2, \ldots, M$, as shown in Fig. 1(a). The coupling strengths at these points are denoted as $g_{31}(x_n) = g_{31}e^{i\alpha x_n}$, $g_{21}(\tilde{x}_m) = g_{21}e^{i\beta \tilde{x}_m}$ with wave vectors α and β for modes in the waveguide A and B, respectively. We take the waveguide A as a channel of a probe field whose transmission is to be observed and the wave-

uide B as a reservoir leading to spontaneous emission via the transition $|2\rangle \leftrightarrow |1\rangle$. To induce EIT, a classical driving field with an angular frequency ν_c and a Rabi frequency Ω_c is applied to the transition $|2\rangle \leftrightarrow |3\rangle$. In Fig. 1(b) we provide a possible experimental realization of our theoretical model. The artificial atom couples to two acoustic waveguides via multiple piezoelectric transducers and each of the transducers can be taken as an individual coupling point [16].

Differently from the recent works in Refs. [30,31], the probe field herein is quantized. In a rotating frame with respect to the frequency ν_c, an effective Hamiltonian of the system in real space reads

$$H_{\text{eff}} = H_a + H_{\text{con}} + H_w + H_I, \tag{1}$$

where

$$H_a = \left(\omega_{21} + \nu_c - \frac{i\gamma_2}{2} \right) |2\rangle\langle 2| + \left(\omega_{31} - \frac{i\gamma_3}{2} \right) |3\rangle\langle 3|,$$

$$H_{\text{con}} = (\Omega_c |3\rangle\langle 2| + \text{H.c.}),$$

$$H_w = \sum_{l=L,R} \int d\tilde{x} b_l^\dagger(\tilde{x}) \left(\nu_c - i f_l \tilde{v}_g \frac{\partial}{\partial \tilde{x}} \right) b_l(\tilde{x})$$

$$- \sum_{l=L,R} f_l \int dx a_l^\dagger(x) \left(i v_g \frac{\partial}{\partial x} \right) a_l(x),$$

$$H_I = \tilde{g}_{31} \sum_{l=L,R} \sum_{n=1}^{N} \int dx \delta(x - x_n)(|3\rangle\langle 1| a_l(x) + \text{H.c.})$$

$$+ \tilde{g}_{21} \sum_{l=L,R} \sum_{m=1}^{M} \int d\tilde{x} \delta(\tilde{x} - \tilde{x}_m)(|2\rangle\langle 1| b_l(\tilde{x}) + \text{H.c.})$$

are the Hamiltonians of the atom, the classical control driving, the waveguides, and the quantized atom-waveguide interactions, respectively. Here we let $\hbar = 1$, $f_R = 1$, $f_L = -1$, and

v_g ($\tilde{v}_g$) is the group velocity of the field in the waveguide A (B). The bosonic annihilation operators a and b with subscripts R and L are for the right- and left-going modes, respectively. The damping rates γ_2 and γ_3 denote the total losses of the atom to the nonwaveguide degrees of freedom [32], and the Dirac δ function indicates the interacting positions. For simplicity, we have assumed that the coupling strengths at each coupling point $\tilde{g}_{3(2)1}$ are identical, and the linear dispersion relation holds in both waveguides. (See the derivation in Appendix A for more details.)

To investigate EIT at the single-photon level, we assume that both the waveguides and the atom are initially prepared in their ground states $|\text{vac}\rangle$ and $|1\rangle$. A single photon is incident from x_1 to x_N such that the scattering eigenstate $|\Psi\rangle$ in the single-excitation subspace [34,35] is

written as

$$|\Psi\rangle = \int dx\big[\phi_R^\alpha(x)a_R^\dagger(x) + \phi_L^\alpha(x)a_L^\dagger(x)\big]|\text{vac}, 1\rangle$$
$$+ \int d\tilde{x}\big[\phi_R^\beta(\tilde{x})b_R^\dagger(\tilde{x}) + \phi_L^\beta(\tilde{x})b_L^\dagger(\tilde{x})\big]|\text{vac}, 1\rangle$$
$$+ e_2|\text{vac}, 2\rangle + e_3|\text{vac}, 3\rangle, \tag{2}$$

where $e_{2(3)}$ is the atomic excitation amplitude of the state $|2(3)\rangle$. According to the interaction Hamiltonian H_I, we plot Fig. 2 to describe the scattering. The coupling at each point acts as an individual δ potential and thus the giant atom can be equivalently treated as a series of cascaded small atoms [5,36]. As such, the probability amplitudes $\phi_{L(R)}^{\alpha(\beta)}(x)$ can be formally written as

$$\phi_R^\alpha(x) = e^{i\alpha x}\left[\theta(x_1 - x) + \sum_{n=1}^{N-1} t_n\theta(x - x_n)\theta(x_{n+1} - x) + t_N\theta(x - x_N)\right], \tag{3a}$$

$$\phi_L^\alpha(x) = e^{-i\alpha x}\left[r_1\theta(x_1 - x) + \sum_{n=2}^{N} r_n\theta(x - x_{n-1})\theta(x_n - x)\right], \tag{3b}$$

$$\phi_R^\beta(\tilde{x}) = e^{i\beta\tilde{x}}\left[\sum_{m=1}^{M-1} \tilde{t}_m\theta(\tilde{x} - \tilde{x}_m)\theta(\tilde{x}_{m+1} - \tilde{x}) + \tilde{t}_M\theta(\tilde{x} - \tilde{x}_M)\right], \tag{3c}$$

$$\phi_L^\beta(\tilde{x}) = e^{-i\beta\tilde{x}}\left[\tilde{r}_1\theta(\tilde{x}_1 - \tilde{x}) + \sum_{m=2}^{M} \tilde{r}_m\theta(\tilde{x} - \tilde{x}_{m-1})\theta(\tilde{x}_m - \tilde{x})\right], \tag{3d}$$

where the Heaviside step function $\theta(x)$ is used to distinguish different intervals. The joint transmission and reflection amplitudes in the intervals of the waveguide $A(B)$ are denoted as $t_n(\tilde{t}_m)$ and $r_n(\tilde{r}_m)$, respectively. Note that these amplitudes represent the overall scatterings under steady states, which include higher-order scatterings resulting from multiple

reflections between every two neighboring coupling points; see Fig. 2(b) for more details.

Substituting Eqs. (1) and (2) into the stationary Schrödinger equation $H_{\text{eff}}|\Psi\rangle = \omega|\Psi\rangle = v_g\alpha|\Psi\rangle$, one can obtain the transmission amplitude t_N and the excitation amplitude e_3:

$$t_N = \frac{\big(\Delta_{31} - \Delta_{32} - \Delta_r^{(M)} + \frac{i\gamma_2}{2} + i\Gamma_{21}^{(M)}\big)\big(\Delta_{31} - \Delta_L^{(N)} + \frac{i\gamma_3}{2}\big) - |\Omega_c|^2}{\big(\Delta_{31} - \Delta_{32} - \Delta_r^{(M)} + \frac{i\gamma_2}{2}\big)\big(\Delta_{31} - \Delta_L^{(N)} + \frac{i\gamma_3}{2} + i\Gamma_{31}^{(N)}\big) - |\Omega_c|^2}, \tag{4a}$$

$$e_3 = \frac{\big(\Delta_{31} - \Delta_{32} - \Delta_r^{(M)} + \frac{i\gamma_2}{2} + i\Gamma_{21}^{(M)}\big)\tilde{g}_{31}\sum_{n=1}^{N} e^{(N-n)i(\Delta_{31}\tau + \phi)}}{\big(\Delta_{31} - \Delta_{32} - \Delta_r^{(M)} + \frac{i\gamma_2}{2} + i\Gamma_{21}^{(M)}\big)\big(\Delta_{31} - \Delta_L^{(N)} + \frac{i\gamma_3}{2} + i\Gamma_{31}^{(N)}\big) - |\Omega_c|^2} \tag{4b}$$

of the probe field, where the detuning frequencies are defined as $\Delta_{31} = \omega - \omega_{31}$ and $\Delta_{32} = v_c - (\omega_{31} - \omega_{21})$. Both of the above equations are affected by the frequency shift

$$\Delta_r^{(M)} = \Gamma_{21}\sum_{m=1}^{M}(M - m)\sin(m\omega_\beta\tilde{\tau}) \tag{5}$$

and the effective decay rate

$$\Gamma_{21}^{(M)} = \Gamma_{21}\sum_{m=1}^{M}\left[\frac{M}{2} + (M - m)\cos(m\omega_\beta\tilde{\tau})\right] \tag{6}$$

induced by the waveguide B, where $\tilde{\tau} = \tilde{d}/\tilde{v}_g$ is a time delay

and $\Gamma_{21} = 2\tilde{g}_{21}^2/\tilde{v}_g$. Interestingly, we find that the spontaneous emission $|2\rangle \leftrightarrow |1\rangle$ can be totally eliminated, when we properly engineer the time delay $\tilde{\tau}$ with respect to a reservoir frequency ω_β. For example, in the case of $M = 2$, the decay rate $\Gamma_{21}^{(2)}$ can be zero when $\omega_\beta\tilde{\tau} = (2k + 1)\pi$, $k \in \mathbb{Z}^+$. Compared to traditional methods, e.g., employing a qubit with multiple Josephson junctions [27,37], unique 3D cavities [38], or nested polariton states [39], our elimination is realized by properly allocating couplings using multiple capacitors or piezoelectric transducers, which simplifies the system. In this way, we can turn a Δ-type atom into a Λ-type one. Hereafter, we assume that this is always the case.
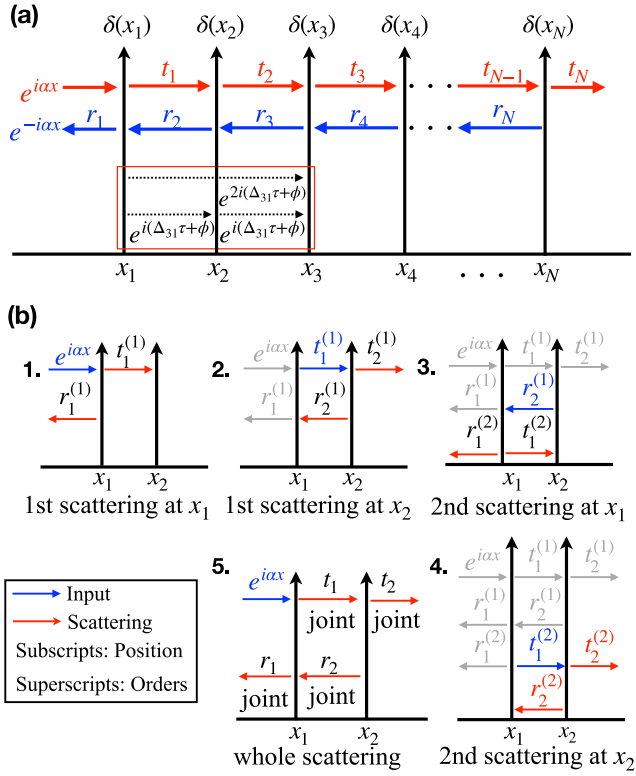
FIG. 2. Schematic of the scattering for the probe field. (a) The total scattering process. In real space, the giant atom behaves as a δ potential at each coupling point x_n. The transmission (reflection) amplitudes t_n (r_n) describe the joint scattering, which contains all order processes due to the multiple reflections occurring at every two coupling points. Since t_N and r_1 represent the scattering occurring at the outermost points, they will contain all the phases accumulated in the previous processes. An example of the accumulated phase for the right-forward propagating process is given in the red box. (b) Schematic of high-order scattering. Here we set $N = 2$ as an example. The input signal is scattered at each coupling point in turn such that scattered right- and left-going modes act as the input of the next scattering process, as shown in subfigures 1–3. The multiple reflections between two coupling points induce higher-order scattering processes, as shown in subfigure 4. Here we take the second-order scattering as an example where the following results can be applied to high-order scattering. Since these scattered fields only contain left- and right-going modes, they can be jointly considered under the steady states, e.g., the joint coefficient t_2 includes $t_2^{(1)}$ and $t_2^{(2)}$, and r_2 includes $r_2^{(1)}$ and $r_2^{(2)}$, as shown in subfigure 5.

In addition, the couplings to the waveguide A induce the frequency-dependent Lamb shift

$$\Delta_L^{(N)} = \Gamma_{31} \sum_{n=1}^{N} (N - n) \sin(n\Delta_{31}\tau + n\phi) \tag{7}$$

and the modified decay rate

$$\Gamma_{31}^{(N)} = \Gamma_{31} \sum_{n=1}^{N} \left[\frac{N}{2} + (N - n) \cos(n\Delta_{31}\tau + n\phi) \right] \tag{8}$$

with $\Gamma_{31} = 2\tilde{g}_{31}^2/v_g$, $\tau = d/v_g$, and $\phi = \omega_{31}\tau$. The first term in the addend of Eq. (8) denotes the joint decay rates attributed

by the N individual coupling points, while the second term is led by the spatial nonlocal couplings. Note that when $N = 2$ and $\Omega_c = 0$, the transmission amplitude t_N in Eq. (4a) reduces to that of a two-level giant atom, which is consistent with these in Refs. [12,16]. Also, the transmission amplitude t_N in Eq. (4a) is modified by Eqs. (7) and (8) with sinusoidals, which indicates that the transmission spectra would be different from those in traditional EIT. Particularly, when $N = 1$, the sinusoidals vanishes such that the decay rate $\Gamma_{31}^{(N)}$ reduces to a constant $\Gamma_{31}/2$, i.e., the giant atom reduces to a small atom, which is consistent with that in Refs. [32,33]. (See Appendix B for more details.)

III. UNCONVENTIONAL EIT

Based on the above results, one can find that the time delay τ is an important parameter which controls the atomic dynamics, such that a reasonable regime of the time delay τ is critical. However, this regime relies on the realistic implements of the giant atom. Actually, besides the acoustic proposal provided in Fig. 1(b), the giant atom can be realized in a microwave proposal, i.e., the acoustic waveguides are replaced with microwave waveguides and the transducers are correspondingly replaced with capacitors [18,31]. The only difference between these proposals lies in that the time delay τ in the acoustic proposal is much greater than that in the microwave proposal. For numerical simulation, we set $N = 2$ for simplicity and use the relative values calculated from the recent experiments. For instance, in the acoustic proposal [7,16,30], the critical parameters are $\omega_{31} \simeq 2\pi \times 4$ GHz, $\Gamma_{31} = 2\pi \times 20$ MHz, $\Omega_c \simeq 2\pi \times 10$ MHz, and $\tau \simeq 160$ns corresponding to $\Gamma_{31}\tau \simeq 20$; In the microwave proposal, these parameters are almost consistent with those in the acoustic proposal, except for $\tau \simeq 0.17$ ns, $\Gamma_{31} \simeq 2\pi \times 20$ MHz corresponding to $\Gamma_{31}\tau \simeq 0.022$ [31]. Therefore, we set the time delay $\tau = 0.05/\Gamma_{31}$ to represent the microwave-coupling regime, and $\tau = 3/\Gamma_{31}$ and $10/\Gamma_{31}$ to represent the acoustic-coupling regime.

In the EIT regime, for simplicity, we plot the transmission spectra $T = |t_N|^2$ in Fig. 3. When the time delay is sufficiently small (i.e., $\tau = 0.05/\Gamma_{31}$) and $\Delta_{31} \ll \omega_{31}$, the Lamb shift $\Delta_L^{(2)}$ and the decay rate $\Gamma_{31}^{(2)}$ are mainly determined by the phase ϕ such that the spectrum has a single absorption peak determined by the frequency ω_{31} as shown in Fig. 3(a), which is consistent with that in Ref. [5]. Particularly, when $\phi = (2k + 1)\pi$, we have $\Delta_L^{(2)} = \Gamma_{31}^{(2)} = 0$ where the system is decoherence-free; i.e., the giant atom is totally decoupled from the waveguide A although there still exists a nonzero coupling Γ_{31}. This is represented by the black dot line in Fig. 3(a). Further, with a given phase $\phi = 200\pi$, we increase the time delay τ so that decoherence-free bands and Lamb-shift-induced absorption peaks appear alternatively and become increasingly dense, as shown in Figs. 3(b)–(d). This is because the absorption peaks with a modified linewidth $\Gamma_{31}^{(2)}$ appear at the single-photon resonance $\Delta_{31} = \Delta_L^{(2)}$. In addition, since the induced transparency occurs at two-photon resonance $\Delta_{31} - \Delta_{32} = 0$, the transparency window $\Gamma_w \simeq |\Omega_c|^2/\Gamma_{31}^{(2)}$ is modified only by the decay rate $\Gamma_{31}^{(2)}$ which depends on the initial phase ϕ, as shown in Fig. 3(b) and the insets in Figs. 3(c) and 3(d). Therefore, the unconventional
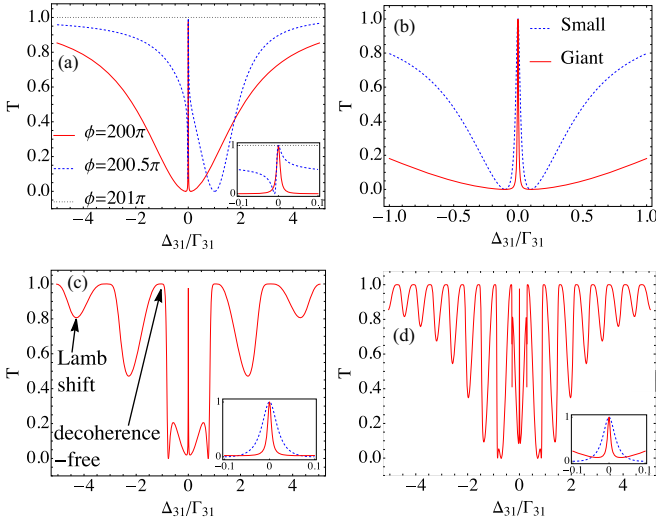
FIG. 3. Transmission spectra of the giant atom in the EIT regime. Parameters used in plotting are $N = 2$, $\Delta_{32} = \gamma_2 = \gamma_3 = 0$, $\Omega_c = 0.1\Gamma_{31}$, and in (a) $\tau = 0.05/\Gamma_{31}$, in (b) $\phi = 200\pi$, $\tau = 0.05/\Gamma_{31}$, in (c) $\phi = 200\pi$, $\tau = 3/\Gamma_{31}$, and in (d) $\phi = 200\pi$, $\tau = 10/\Gamma_{31}$. (a) With the extremely small time delay τ, the spectra have only one peak since where both the Lamb shift $\Delta_{31}^{(2)}$ and decay rate $\Gamma_{31}^{(2)}$ are mainly determined by the phase ϕ. (b) Compared to small atoms, the transparent window of the giant atom $\Gamma_w \simeq |\Omega_c|^2/\Gamma_{31}^{(2)}$ is modified by the phase ϕ. In (c) and (d), we show the unconventional EIT spectra with increased time delays τ when the phase ϕ is fixed. In both cases, $\Delta_{31}\tau$ dominate the variations of $\Delta_{31}^{(2)}$ and $\Gamma_{31}^{(2)}$ such that absorption peaks (arrow to Lamb shift) and transparent subpeaks (arrow to decoherence-free) appear alternately. The blue dashed lines in the insets represent the small atom case.
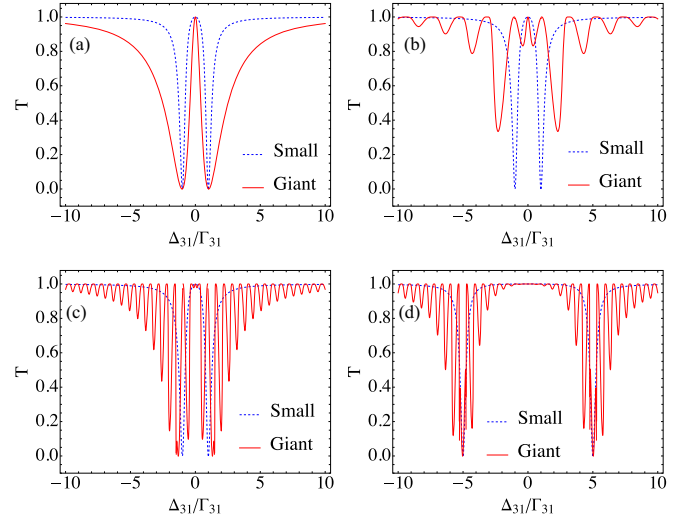
FIG. 4. Transmission spectra of the giant atom in the ATS regime. Parameters used in plotting are $N = 2$, $\Delta_{32} = \gamma_2 = \gamma_3 = 0$, $\phi = 200\pi$, and in (a) $\Omega_c = \Gamma_{31}$, $\tau = 0.05/\Gamma_{31}$, in (b) $\Omega_c = \Gamma_{31}$, $\tau = 3/\Gamma_{31}$, in (c) $\Omega_c = \Gamma_{31}$, $\tau = 10/\Gamma_{31}$, and in (d) $\Omega_c = 5\Gamma_{31}$, $\tau = 10/\Gamma_{31}$. In the ATS regime, the multiple peaks are reflected on two dressed states. Blue dot lines represent those in the case of small atoms ($N = 1$). (a) The linewidths of dressed states are clearly modified by $\Gamma_{31}^{(2)}$ with a small time delay τ. In (b) and (c), analogous to EIT, as the time delay τ increases, the multiple peaks become dense. In particular, there is an enormous difference between the two curves in (b) because the $\Delta_L^{(2)}$ changes the positions of two dressed states when the time delay τ is sufficiently large. (d) Compared to (c), when the time delay τ is fixed, the larger Rabi frequency Ω_c dominates the dressed states such that two main absorption peaks split into several subpeaks due to the small modification on the Lamb shift $\Delta_L^{(2)}$.

EIT can be observed when the time delay between two neighboring coupling points is comparable to the relaxation time $1/\Gamma_{31}$.

Note that by increasing the Rabi frequency Ω_c, similar solutions can also be found in the Autler-Townes splitting (ATS) [40–44] regime, as shown in Fig. 4. However, since the single-photon resonance (i.e., $\Delta_{31} = \Delta_L^{(2)}$) in the ATS regime corresponds to dressed states induced by a large Rabi frequency Ω_c, the periodicity of $\Delta_L^{(2)}$ is determined by the modulation on the dressed states. This means that both the Rabi frequency Ω_c and the Lamb shift $\Delta_L^{(2)}$ jointly affect both the positions and linewidths of the dressed states. When the time delay τ is sufficiently small, compared to the small atoms, the linewidth is still clearly modified by the decay rate $\Gamma_{31}^{(2)}$ mainly determined by the phase ϕ, as shown in Fig. 4(a). Analogous to EIT, the absorption peaks become dense as τ increases, as shown in Figs. 4(b) and 4(c). However, there exists an obvious difference between the two curves in Fig. 4(b). This is because the $\Delta_L^{(2)}$ changes the positions of two dressed states when the time delay τ is sufficiently large. With further increasing the Rabi frequency Ω_c, e.g., $\Omega_c = 5\Gamma_{31}$, two dressed states split into several subpeaks due to the modification of the Lamb shift $\Delta_L^{(2)}$, as shown in Fig. 4(d).

Another interesting point is that a strong modification can be obtained by increasing the number of the coupling points. Here, we show this by comparing the transmission spectra in the ATS regime between $N = 2$ and $N = 3$. Since the

maximum values of $\Delta_L^{(3)} = 4\Gamma_{31} \sin(\Delta_{31}\tau + \phi) \cos^2(\frac{\Delta_{31}\tau + \phi}{2})$ and $\Gamma_{31}^{(3)} = 2\Gamma_{31}[\frac{1}{2} + \cos(\Delta_{31}\tau + \phi)]^2$ are greatly enhanced compared to $\Delta_L^{(2)} = \Gamma_{31} \sin(\Delta_{31}\tau + \phi)$ and $\Gamma_{31}^{(2)} = \Gamma_{31}[1 + \cos(\Delta_{31}\tau + \phi)]$, the variations of the spectra with $N = 3$ is more sensitive to the detuning Δ_{31} and the time delay τ, as shown in Fig. 5. As the time delay τ increases, the multiple absorption peaks also become dense in the spectra with $N = 3$, as shown in Figs. 5(a)–5(c).

However, the on-resonance absorption efficiency greatly increases at the single-photon resonance when $N = 3$. This is because a large N leads to an enhancement of the modified decay rate $\Gamma_{31}^{(N)}$ when Δ_{31} and τ are fixed, which means that the effective coupling between the atom and the waveguide is amplified. Moreover, when the Rabi frequency Ω_c is comparable to Γ_{31}, there exists a transition from the transparency to the absorption at two dressed states $\Delta_{31} = \pm\Omega_c$, i.e., $|t_3|^2 \simeq 0$ and $|t_2|^2 \simeq 0.995$ in Fig. 5(b), and $|t_3|^2 \simeq 0.37$ and $|t_2|^2 \simeq 0.919$ in Fig. 5(c). This is because the increasing N changes the bands when decoherence is suppressed. However, as Ω_c increases (e.g., $\Omega_c = 5\Gamma_{31}$), two spectra show a good agreement at $\Delta_{31} = \pm5\Omega_c$, as shown in Fig. 5(d) where $|t_3|^2 \simeq 0.054$ and $|t_2|^2 \simeq 0.018$. This is because the changes of two dressed states induced by the Lamb shift $\Delta_L^{(N)}$ is too small compared to that induced by a large Rabi frequency Ω_c.
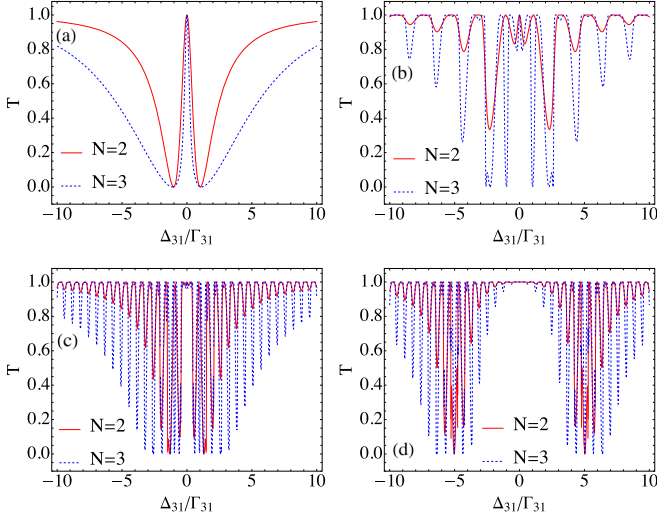
FIG. 5. Transmission spectra of the giant atom when $N = 2$ and $N = 3$ in the ATS regime. Parameters used in plotting are $\Delta_{32} = \gamma_2 = \gamma_3 = 0$, $\phi = 200\pi$, and in (a) $\Omega_c = \Gamma_{31}$, $\tau = 0.05/\Gamma_{31}$, in (b) $\Omega_c = \Gamma_{31}$, $\tau = 3/\Gamma_{31}$, in (c) $\Omega_c = \Gamma_{31}$, $\tau = 10/\Gamma_{31}$, and in (d) $\Omega_c = 5\Gamma_{31}$, $\tau = 10/\Gamma_{31}$. A stronger modulation can be realized by increasing the number of coupling points N. (a) When the time delay τ is small enough, two spectra are approximately the same and the positions of two dressed states occur at $\Delta_{31} = \pm\Omega_c$. (b), (c) As the time delay τ increases, the multipeak property becomes much clearer in both spectra. However, there exists a transition from transparency to absorption at two dressed states $\Delta_{31} = \pm\Omega_c$ between the spectra $N = 3$ and $N = 2$, i.e., in (b) $|t_3|^2 \simeq 0$ and $|t_2|^2 \simeq 0.995$, in (c) $|t_3|^2 \simeq 0.37$ and $|t_2|^2 \simeq 0.919$. (d) Compared to (c), for a fixed time delay τ, the above transition at two dressed states $\Delta_{31} = \pm5\Omega_c$ is vanished by a larger Rabi frequency Ω_c, i.e., $|t_3|^2 \simeq 0.054$ and $|t_2|^2 \simeq 0.018$.

IV. STANDING WAVE INSIDE THE SCATTERING INTERVALS

In Sec. III we have discussed the unconventional EIT with multipeak properties which are governed by the Lamb shifts $\Delta_{31}^{(N)}$ (8) and the effective decay rates $\Gamma_{31}^{(N)}$ (9). The resulting sinusoidal form of Eqs. (7) and (8) is caused by the boundary condition of standing waves, i.e., the interference between bidirectional propagating waves form standing waves inside each scattering interval. This can be treated as the time-delayed coherent feedback [45] where the output signal is guided back to the system through a transmission line after a time delay and each round of feedback can be considered as that the input interacts with the system at another position. The obtained results show that the final output spectra can also exhibit a multiple-peak property if the modes in the transmission line are discrete.

From a different point of view, the giant atom acts as mirrors cutting the entire waveguide into several *cascaded cavities*. For a right-forward propagating field, the incident single photon picks up a phase $e^{ni(\Delta_{31}\tau+\phi)}$ when it passes through a cavity formed by two coupling points. Correspondingly, the photon accumulates a conjugate phase $e^{-ni(\Delta_{31}\tau+\phi)}$ during the propagation in the opposite direction. For instance, the photon accumulates a phase $e^{i(\Delta_{31}\tau+\phi)}$ from x_1 to x_2; From x_1 to x_3, the photon accumulates phases $2e^{i(\Delta_{31}\tau+\phi)}$ and $e^{2i(\Delta_{31}\tau+\phi)}$. The phase $2e^{i(\Delta_{31}\tau+\phi)}$ results from the sum of two individual phases accumulated in $x_1 \to x_2$ and $x_2 \to x_3$, while $e^{2i(\Delta_{31}\tau+\phi)}$ results from the phase directly accumulated in $x_1 \to x_3$, as shown in the red box of Fig. 2. This process exists only in the giant atom, and it is described by the joint transmission and reflection amplitudes in the scattering intervals. To show this process, we plot the scattering spectra $\tilde{T} = |t_1|^2$ and $\tilde{R} = |r_2|^2$ with

$$t_1 = \frac{\left(\Delta_{31} - \Delta_{32} + \frac{i\gamma_2}{2}\right)\left(\Delta_{31} - \frac{\Delta_L^{(2)}}{2} + \frac{i\gamma_3}{2} + \frac{i\Gamma_{31}^{(2)}}{2}\right) - |\Omega_c|^2}{\left(\Delta_{31} - \Delta_{32} + \frac{i\gamma_2}{2}\right)\left(\Delta_{31} - \Delta_L^{(2)} + \frac{i\gamma_3}{2} + i\Gamma_{31}^{(2)}\right) - |\Omega_c|^2},\tag{9a}$$

$$r_2 = -\frac{i\Gamma_{31}}{2}\frac{\left[e^{i(\Delta_{31}\tau+\phi)} + e^{2i(\Delta_{31}\tau+\phi)}\right]\left(\Delta_{31} - \Delta_{32} + \frac{i\gamma_2}{2}\right)}{\left(\Delta_{31} - \Delta_{32} + \frac{i\gamma_2}{2}\right)\left(\Delta_{31} - \Delta_L^{(2)} + \frac{i\gamma_3}{2} + i\Gamma_{31}^{(2)}\right) - |\Omega_c|^2}\tag{9b}$$

inside the intervals when $N = 2$ in Fig. 6. As we mentioned before, the standing wave comes from the interference between bidirectional modes such that it requires a nonzero $\tilde{T}$ and $\tilde{R}$. In addition, the normalization property of wave functions requires $\tilde{T} + \tilde{R} = 1$ in principle. Therefore, those unnormalized points of $\tilde{T} + \tilde{R}$ should be attributed to the interference between the bidirectional propagating modes inside the scattering intervals. The only difference between these two terms lies in that there exist multiple reflections inside the scattering interval, as shown in Fig. 2(b). The multiple reflections make the emitted fields inside the interval coherent but in opposite directions, thus these fields could interfere with each other (both the enhancement and destruction occur). On the contrary, $T + R$ represents the scattering outside the outermost coupling points, such that the emitted fields are

unidirectional, i.e., the transmission is right-forward (denoted by T) and the reflection is left-forward (denoted by R). Therefore, there does not exist a field in opposite direction to interfere with the emitted fields. This difference makes $\tilde{T} + \tilde{R} \neq 1$. Hence, the interference between bidirectional propagating waves attributes to the sinusoidal form such that the standing waves therein lead to the multiple peaks in Figs. 3 and 4.

V. TIME-DELAYED MASTER EQUATION

In Sec. III we have discussed the unconventional EIT induced by the nonlocal couplings, which behaves as the scattering spectra possessing multiple peaks. Actually, it also describes a non-Markovian effect satisfying a time-delayed
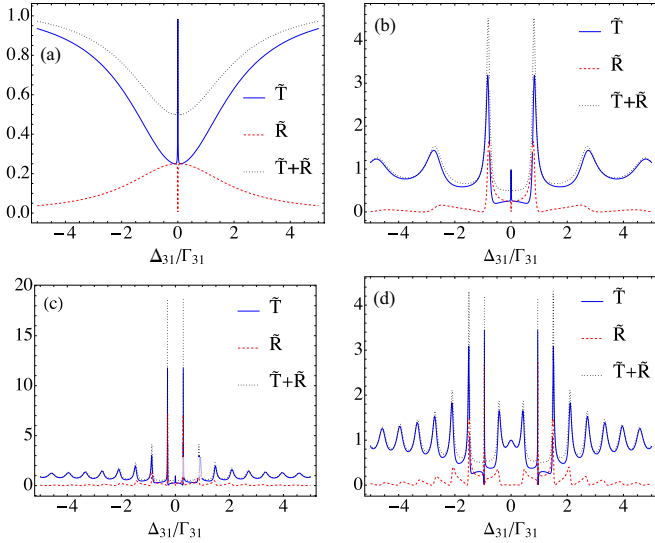
FIG. 6. Transmission and reflection spectra inside the scattering interval. The parameters in the plots are $N = 2$, $\gamma_2 = \gamma_3 = \Delta_{32} = 0$, $\phi = 200\pi$, and in (a) $\Omega_c = 0.1\Gamma_{31}$, $\tau = 0.05/\Gamma_{31}$, in (b) $\Omega_c = 0.1\Gamma_{31}$, $\tau = 3/\Gamma_{31}$, in (c) $\Omega_c = 0.1\Gamma_{31}$, $\tau = 10/\Gamma_{31}$, and in (d), $\Omega_c = \Gamma_{31}$, $\tau = 10/\Gamma_{31}$. $\tilde{T} + \tilde{R}$ (black dashed lines) is not always normalized except for two-photon resonance. The unnormalized points indicate an enhancement of interference between bidirectional modes, while the normalized points $\tilde{T} = 1$ and $\tilde{R} = 0$ ($\tilde{T} = 0$ and $\tilde{R} = 1$) correspond to the local maximum (minimum) of interference.

master equation

$$\dot{\rho}_a^q(t) = -i\big[V^c(t), \rho_a^q(t)\big] + \mathcal{L}_{\text{Loc}}\rho_a^q(t)$$
$$+ \sum_{n=1}^{N} \mathcal{L}_D^A \rho_a^q(t - n\tau) + \sum_{m=1}^{M} \mathcal{L}_D^B \rho_a^q(t - m\tilde{\tau}), \quad (10)$$

where $\rho_a^q(t)$ is the reduced density operator of the atom. Here the superscript q labels the quantities in the full quantum case, which distinguishes the quantities with a superscript c in a classical theory, i.e., without considering the quantized atom-waveguide interactions. The interaction Hamiltonian

$V^c(t)$ reads

$$V^c(t) = \left(\sum_{n=1}^{N} \Omega_p e^{-i\Delta_{31}t + i\alpha x_n} |3\rangle\langle 1| + \text{H.c.} \right)$$
$$+ (\Omega_c e^{-i\Delta_{32}t} |3\rangle\langle 2| + \text{H.c.}) \quad (11)$$

denoting the evolution under the probe field labeled by Ω_p and the control field labeled by Ω_c. The superoperator

$$\mathcal{L}_{\text{Loc}}\rho_a^q(t) = \sum_{i=2,3} \gamma_i^\phi \mathcal{D}[|i\rangle\langle i|]\rho_a^q(t) + \gamma_{32}\mathcal{D}[|2\rangle\langle 3|]\rho_a^q(t)$$
$$+ (\gamma_{31} + N\Gamma_{31})\mathcal{D}[|1\rangle\langle 3|]\rho_a^q(t)$$
$$+ M\Gamma_{21}\mathcal{D}[|1\rangle\langle 2|]\rho_a^q(t) \quad (12)$$

in the first line describes a local dissipation related to the nonwaveguide decoherence rate $\gamma_{31(2)}$ and the pure dephasing rate $\gamma_{2(3)}^\phi$. The summations in the second line of Eq. (10)

$$\mathcal{L}_D^A \rho_a^q(t - n\tau) = -i\Delta_L'[|3\rangle\langle 3|, \rho_a^q(t - n\tau)]$$
$$+ 2\Gamma_{31}'\mathcal{D}[|1\rangle\langle 3|]\rho_a^q(t - n\tau), \quad (13a)$$
$$\mathcal{L}_D^B \rho_a^q(t - m\tilde{\tau}) = -i\Delta_r'[|2\rangle\langle 2|, \rho_a^q(t - m\tilde{\tau})]$$
$$+ 2\Gamma_{21}'\mathcal{D}[|1\rangle\langle 2|]\rho_a^q(t - m\tilde{\tau}), \quad (13b)$$

respectively, represent the nonlocal evolution related to the waveguide A and B with the damping rates $\Gamma_{31}' = \Gamma_{31}(N - n)\cos(n\omega_{31}\tau)$ and $\Gamma_{21}' = \Gamma_{21}(M - m)\cos(\omega_{21}\tilde{\tau})$, and the frequency shifts $\Delta_L' = \Gamma_{31}(N - n)\sin(n\omega_{31}\tau)$ and $\Delta_r' = \Gamma_{21}(M - m)\sin(\omega_{21}\tilde{\tau})$. These delayed terms describe a non-Markovian effect, i.e., the waveguides are not memoryless. Here $\mathcal{D}[O]\rho(t)$ is the standard Lindblad superoperator for an arbitrary operator O. (See the derivation in Appendix C.)

The time-delayed differential equation (11) can be expanded in a matrix element form. Here we focus on two coupled elements ρ_{31}^q and ρ_{21}^q since ρ_{31}^q represents the excitation and dispersion of the atom for the probe field and it is equivalent to the excitation e_3 in Eq. (4b) in real-space scattering method. The equations of motion with respect to ρ_{21}^q and ρ_{31}^q read

$$\dot{\bar{\rho}}_{21}^q(t) = i\left(\Delta_{31} - \Delta_{21} + i\Gamma_{21}\frac{M}{2} + \frac{i\gamma_2}{2}\right)\bar{\rho}_{21}^q(t) - \Gamma_{21}\sum_{m=1}^{M}(M - m)e^{mi\omega_\beta\tilde{\tau}}\bar{\rho}_{21}^q(t - m\tilde{\tau}) - i\Omega_c^*\bar{\rho}_{31}^q(t), \quad (14a)$$

$$\dot{\bar{\rho}}_{31}^q(t) = i\left(\Delta_{31} + i\Gamma_{31}\frac{N}{2} + \frac{i\gamma_3}{2}\right)\bar{\rho}_{31}^q(t) - \Gamma_{31}\sum_{n=1}^{N}(N - n)e^{ni(\Delta_{31}\tau + \phi)}\bar{\rho}_{31}^q(t - n\tau) - i\Omega_c\bar{\rho}_{21}^q(t) - i\sum_{n=1}^{N}\Omega_p e^{i\alpha x_n}, \quad (14b)$$

where $\gamma_2 = \gamma_2^\phi$ and $\gamma_3 = \gamma_{31} + \gamma_{32} + \gamma_3^\phi$ are the total loss rates to the nonwaveguide degrees of freedom, as the same as we defined in Eq. (1). Here, $\bar{\rho}_{21}^q(t) = \rho_{21}^q(t)e^{i(\Delta_{31} - \Delta_{32})t}$ and $\bar{\rho}_{31}^q(t) = \rho_{31}^q(t)e^{i\Delta_{31}t}$ denote the slowly varying quantities. In the derivation, we have considered $\omega - \nu_c = \omega_\beta$ and the atom evolves adiabatically such that the populations at the level $|i\rangle$

remain the same, i.e., $\rho_{11}^q(0) = \rho_{11}^q(t) = 1$, $\rho_{22}^q(0) = \rho_{22}^q(t) = \rho_{33}^q(0) = \rho_{33}^q(t) = 0$ [46]. Since we are interested in the excitation properties under the steady states, the above coupled equations can be solved by performing a Fourier transformation and let the frequency introduced by the transformation be zero. Finally, the steady-state solution reads

$$\tilde{\rho}_{31}^q = \frac{\sum_{n=1}^{N} 2\pi\delta(0)\Omega_p e^{(N-n)i(\Delta_{31}\tau + \phi)}\left(\Delta_{31} - \Delta_{32} - \Delta_r^{(M)} + i\Gamma_r^{(M)} + \frac{i\gamma_2}{2}\right)}{\left(\Delta_{31} - \Delta_{32} - \Delta_r^{(M)} + i\Gamma_r^{(M)} + \frac{i\gamma_2}{2}\right)\left(\Delta_{31} - \Delta_L^{(N)} + i\Gamma_{31}^{(N)} + \frac{i\gamma_3}{2}\right) - |\Omega_c|^2}. \quad (15)$$

Note that Eq. (15) is consistent with the excitation e_3 (4b) under the replacement $\tilde{g}_{31} \to \Omega_p$. Notably, the time delayed terms induced by the spatial nonlocality $\mathcal{L}_D^A \rho_a^q(t - n\tau)$ and $\mathcal{L}_D^B \rho_a^q(t - m\tilde{\tau})$ are now embedded in the sinusoidals of Eqs. (7) and (8), such that the non-Markovian effect in frequency domain behaves as the dependence of $\Gamma_{31}^{(N)}$ on the input frequency Δ_{31} which exhibits a multipeak property in transmission spectra (cf. Figs. 3 and 4). Besides, this type of non-Markovian effects results from the inherent nonlocalities rather than the spectral property of interacting environments, which is different from common non-Markovian dynamics [47–49].

VI. FURTHER DISCUSSION Of THE MASTER EQUATION

Traditionally, the EIT phenomenon is commonly described by a master equation under Born-Markovian approximation without considering the quantized atom-waveguide interactions [26]. However, this treatment is not applicable to giant atoms. In this section, we start from this type of master equation and show why the quantized interactions are needed in giant atoms in Sec. VI A. We then discuss the validity of Markovian approximation in Sec. VI B.

A. Comparison with the master equation used in Ref. [31]

In Ref. [31] the authors also consider EIT in a Λ-type transmon qubit coupled to a waveguide at multiple points but the observed results show that there exists a discrepancy between the data and the fit calculated by a master equation without considering the quantized atom-waveguide interactions in Fig. 8 of Ref. [31], although they have applied a rotation to take the phases into account. Given this, we provide the following derivation to show why this type of master equation is not suitable for giant atoms.

According to the Ref. [31], the dynamics of the λ-type giant atom is governed by the Lindblad master equation

$$\dot{\rho}_a^c(t) = -i[V^c(t), \rho_a^c(t)] + \mathcal{L}_{\text{loc}}^0 \rho_a^c(t), \quad (16)$$

where

$$\mathcal{L}_{\text{loc}}^0 \rho_a^c(t) = \sum_{i=2,3} \gamma_i^\phi \mathcal{D}[|i\rangle\langle i|]\rho_a^c(t) + \gamma_{32}\mathcal{D}[|2\rangle\langle 3|]\rho_a^c(t)$$
$$+ (\gamma_{31} + \Gamma_{31})\mathcal{D}[|1\rangle\langle 3|]\rho_a^c(t).$$

Here, the symbols are as same as those we defined in Sec. V, and Γ_{31} is introduced to phenomenally consider the decoherence to the waveguide A. Following the same procedure in Sec. V, the solution reads

$$\tilde{\rho}_{31}^c = \frac{\sum_{n=1}^N 2\pi\delta(0)\Omega_p e^{(N-n)i(\Delta_{31}\tau+\phi)}\left(\Delta_{31} - \Delta_{32} + \frac{i\gamma_2}{2}\right)}{\left(\Delta_{31} - \Delta_{32} + \frac{i\gamma_2}{2}\right)\left(\Delta_{31} + \frac{i\Gamma_{31}}{2} + \frac{i\gamma_2}{2}\right) - |\Omega_c|^2}. \quad (17)$$

In contrast to the excitation e_3 (4b), the decay rate Γ_{31} here is a constant since it is phenomenally introduced without considering the multiple-point couplings between the atom and the waveguide A, such that it cannot induce the frequency-dependent Lamb shift and modified decay rate [cf. Eqs. (7)
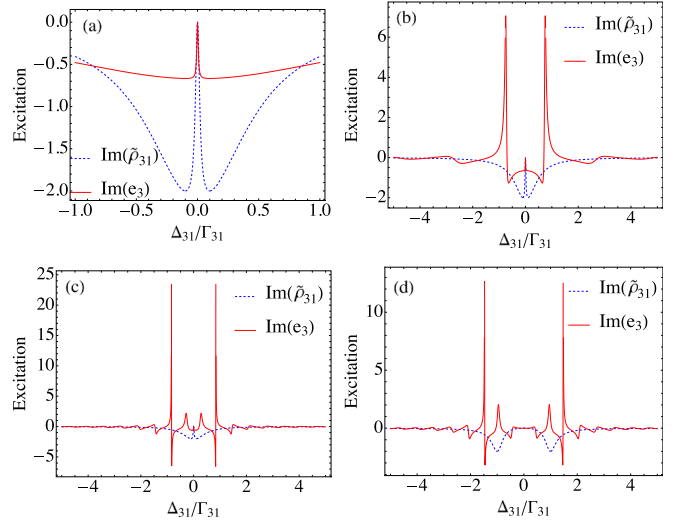

FIG. 7. The excitation spectra of the giant atom obtained by the semiclassical master equation and by the real-space method when $N = 2$. Parameters used in plotting are $\Delta_{32} = \gamma_2 = \gamma_3 = 0$, $\phi = 200\pi$, and in (a) $|\Omega_c| = 0.1\Gamma_{31}$, $\tau = 0.05/\Gamma_{31}$, in (b) $|\Omega_c| = 0.1\Gamma_{31}$, $\tau = 3/\Gamma_{31}$, in (c) $|\Omega_c| = 0.1\Gamma_{31}$, $\tau = 10/\Gamma_{31}$, and in (d) $|\Omega_c| = \Gamma_{31}$, $\tau = 10/\Gamma_{31}$. Here the superscript c in Eq. (17) is neglected for brevity. With the absence of effective decay rate $\Gamma_{31}^{(N)}$, the master equation always provides standard EIT or ATS spectra, as plotted as blue dotted lines. However, as the time delay τ increases, the multipeak property becomes much denser in the full quantum theory, as plotted as red solid lines.

and (8)]. As a result, $\tilde{\rho}_{31}^c$ cannot exhibit a multipeak absorption spectra. To show this, we compare the excitation properties between $\tilde{\rho}_{31}^c$ (17) and e_3 (4b) in Fig. 7, where both the factors $\Omega_p \sum_{n=1}^N e^{(N-n)i(\Delta_{31}\tau+\phi)}$ and $\tilde{g}_{31} \sum_{n=1}^N e^{(N-n)i(\Delta_{31}\tau+\phi)}$ are divided in normalization. One can see that this type of master equation always provides standard EIT or ATS spectra, as plotted in blue dotted lines. However, as the time delay τ increases, the multipeak property of e_3 becomes much denser, as plotted in solid red lines.

The differences in Fig. 7 indicate that the this type of master equation cannot well explain the special features of giant atoms. This is because the quantized interaction between the atom and the waveguide is neglected in this theory (see Appendix C for more details). Indeed, if a classical input enters the system from a waveguide, it can be decomposed into two parts: (1) classical amplitudes denoted by Rabi frequencies and (2) quantized noise input resulting from the quantized system-waveguide coupling, which is denoted by creation and annihilation operators of the waveguide [50–53]. Therefore, if the classical amplitude with multiple-point couplings is considered, the quantized noise input should also be considered in a similar way. Although in most cases, the theory without considering the second point (2) is in good agreements with experiments, it does not apply to giant atoms since the multipeak properties and non-Markovian effects therein are quantum effects that requires point (2).

B. The validity of Markovian approximation

In Ref. [5] the authors analyze the dynamics of a giant atom utilizing a full-quantum master equation under

Markovian approximation. The obtained results show that the Lamb shifts and modified decay rates only depend on the atomic frequencies, i.e., the $\Delta_{31}\tau$ part is missing in both $\Delta_L^{(N)}$ (8) and $\Gamma_{31}^{(N)}$ (9). As we discussed in Sec. III, this treatment is valid only when the time delay τ is so small that it hardly affects the dynamics of the atom. Indeed, Markovian approximation is a local transformation which manually eliminates the nonlocality, i.e., if we perform a Markovian approximation $\rho_a^q(t - n\tau) \to \rho_a^q(t)$ and $\rho_a^q(t - m\tilde{\tau}) \to \rho_a^q(t)$, Eq. (10) then becomes

$$\dot{\rho}_a^{qm}(t) = -i\big[V^c(t), \rho_a^{qm}(t)\big] + \mathcal{L}_{\text{Loc}}^{qm}\rho_a^{qm}(t) \qquad (18)$$

with

$$\mathcal{L}_{\text{Loc}}^{qm}\rho_a^{qm}(t) = \sum_{\text{i}=2,3} \gamma_{\text{i}}^{\phi}\mathcal{D}[|\text{i}\rangle\langle\text{i}|]\rho_a^{qm}(t)$$
$$+ \gamma_{32}\mathcal{D}[|2\rangle\langle3|]\rho_a^{qm}(t) + \gamma_{31}\mathcal{D}[|1\rangle\langle3|]\rho_a^{qm}(t)$$

$$+ 2\Gamma_{31}^{qm}\mathcal{D}[|1\rangle\langle3|]\rho_a^{qm}(t) - i\Delta_L^{qm}\big[|3\rangle\langle3|, \rho_a^{qm}(t)\big]$$
$$+ 2\Gamma_{21}^{qm}\mathcal{D}[|1\rangle\langle2|]\rho_a^{qm}(t) - i\Delta_r^{qm}\big[|2\rangle\langle2|, \rho_a^{qm}(t)\big],$$

where

$$\Gamma_{31}^{qm} = \Gamma_{31} \sum_{n=1}^{N} \left[\frac{N}{2} + (N - n)\cos(n\phi)\right], \qquad (19a)$$

$$\Delta_L^{qm} = \Gamma_{31} \sum_{n=1}^{N} (N - n)\sin(n\phi), \qquad (19b)$$

$$\Gamma_r^{qm} = \Gamma_{21} \sum_{m=1}^{M} \left[\frac{M}{2} + (M - m)\cos(m\omega_{21}\tilde{\tau})\right], \quad (19c)$$

$$\Delta_r^{qm} = \Gamma_{21} \sum_{m=1}^{M} (M - m)\sin(m\omega_{21}\tilde{\tau}). \qquad (19d)$$

Here the superscript qm means the quantities derived from a quantum theory under Markovian approximation. Following the procedure we used before, the solution reads

$$\tilde{\rho}_{31}^{qm} = \frac{\sum_{n=1}^{N} 2\pi\delta(0)\Omega_p e^{(N-n)i(\Delta_{31}\tau + \phi)}\big(\Delta_{31} - \Delta_{32} - \Delta_r^{qm} + i\Gamma_r^{qm} + \frac{i\gamma_2}{2}\big)}{\big(\Delta_{31} - \Delta_{32} - \Delta_r^{qm} + i\Gamma_r^{qm} + \frac{i\gamma_2}{2}\big)\big(\Delta_{31} - \Delta_L^{qm} + i\Gamma_{31}^{qm} + \frac{i\gamma_3}{2}\big) - |\Omega_c|^2}. \qquad (20)$$

One can see that the frequency-dependent properties herein are localized at the atomic frequencies, as same as those in Ref. [5]. In the real-space scattering method, the Markovian approximation behaves as $e^{i\alpha x} \to e^{i\omega_{31}x/v_g}$ [54,55], and one can obtain the excitation amplitude e_3 having a similar form (20).

Comparing Eq. (10) and Eq. (18), one can conclude that the dynamics under the quantized atom-waveguide interaction is governed by the decay of N individual points and the interferences between these points, respectively. The improper using of Markovian approximation destroys the non-Markovian retarding effects that are supposed to be present in the system.

VII. CONCLUSION

In conclusion, we discovered unconventional EIT and ATS in a single giant atom. Also, we presented a time-delayed master equation approach to observing the unconventional EIT and the corresponding results are consistent with those calculated by the existing real-space scattering method. This interesting phenomenon is a typical quantum effect, and our theory indicates that it cannot be characterized in the absence of quantized atom-waveguide interactions [30,31]. To observe it in an experiment, the time delay between two neighboring coupling points must be comparable to the relaxation time, and this is why it has not been experimentally observed so far. Also, the physics behind this phenomenon is the inherent nonlocality of giant atoms which leads to the standing waves in space and retardations in time. More importantly, in a recent review [23], giant atoms are defined by the ratio between the atomic size and the wavelength of the interacting fields, however, this definition is improper. When a transmon qubit couples to the acoustic waves via a single interdigitated

transducer [30], the transmon qubit is "giant" in this sense. However, the observed phenomenon is as same as those in small atoms. Thus, giant atoms should be defined as atoms who are coupled to the waveguides at multiple points, since the nonlocality resulting from this structure is the core for the all of unconventional effects therein.

The proposed time-delayed master equation describes the non-Markovian dynamics of the giant atom in time domain, based on which we can further consider quantum control of giant atoms. Also, our work has established a theoretical basis for giant atoms, which can be used to explore possible applications in future quantum devices, such as filters [56–58], switches [3,33], memories [59], slowing/stopping light [60–62], lasers without inversion [63–65], and frequency convertors [34]. Besides these traditional applications, a more interesting direction is utilizing giant atoms to design quantum sensors [53]. In Ref. [53] the authors find that the giant-cavity (i.e., cavities couple to the waveguide with multipoint couplings) -based proposal can build up an inherent nonreciprocal coupling due to the multipoint coupling structure, and the sensing performance can be greatly enhanced compared to the small-cavity-based proposal. Especially, their output noise can remain at the shot noise level. These results show great values of giant atoms in quantum sensing, therefore, a future direction is to apply giant atoms to quantum sensing.

APPENDIX A: MATHEMATICS ON DERIVATIONS OF HAMILTONIAN AND SCATTERING AMPLITUDES

The original Hamiltonian of the system in Fig. 1 is given by

$$
H_o = \omega_{21}|2\rangle\langle2| + \omega_{31}|3\rangle\langle3| + \int d\alpha\,\omega_\alpha a_\alpha^\dagger a_\alpha
$$

$$
+ \int d\beta\,\omega_\beta b_\beta^\dagger b_\beta + (\Omega_c e^{-iv_c t}|3\rangle\langle2| + \text{H.c.})
$$

$$
+ \sum_{n=1}^N \int d\alpha[g_{31}(x_n)|3\rangle\langle1|a_\alpha + \text{H.c.}]
$$

$$
+ \sum_{m=1}^M \int d\beta[g_{21}(\tilde{x}_m)|2\rangle\langle1|b_\beta + \text{H.c.}], \qquad (A1)
$$

where we define the coupling strengths as $g_{31}(x_n) = g_{31}e^{i\alpha x_n}$ and $g_{21}(\tilde{x}_m) = g_{21}e^{i\beta\tilde{x}_m}$. Rotating the system with $U = \exp(iv_c t|2\rangle\langle2| + iv_c t\int d\beta\, b_\beta^\dagger b_\beta)$, we then can obtain a time-independent Hamiltonian

$$
H = (\omega_{21} + v_c)|2\rangle\langle2| + \omega_{31}|3\rangle\langle3| + \int d\alpha\,\omega_\alpha a_\alpha^\dagger a_\alpha
$$

$$
+ \int d\beta\,(\omega_\beta + v_c)b_\beta^\dagger b_\beta + (\Omega_c|3\rangle\langle2| + \text{H.c.})
$$

$$
+ \sum_{n=1}^N \int d\alpha[g_{31}(x_n)|3\rangle\langle1|a_\alpha + \text{H.c.}]
$$

$$
+ \sum_{m=1}^M \int d\beta[g_{21}(\tilde{x}_m)|2\rangle\langle1|b_\beta + \text{H.c.}]. \qquad (A2)
$$

Here we assume that the entire frequency range of interest is far away from the cutoff frequencies of the waveguides such that the linear dispersion relation holds, i.e., $\omega_\alpha = v_g\alpha$, $\omega_\beta = \tilde{v}_g\beta$. Also, only modes in a very narrow frequency interval around ω_{31} and ω_{21} can efficiently interact with the atom, and thus the waveguide modes can be treated as two distinct ones [32], i.e.,

$$
\int d\alpha\,\omega_\alpha a_\alpha^\dagger a_\alpha = \int d\alpha_R\,\omega_{\alpha_R} a_{\alpha_R}^\dagger a_{\alpha_R}
$$

$$
+ \int d\alpha_L\,\omega_{\alpha_L} a_{\alpha_L}^\dagger a_{\alpha_L}, \qquad (A3a)
$$

$$
\int d\beta\,(\omega_\beta + v_c)b_\beta^\dagger b_\beta = \int d\beta_R\,(\omega_{\beta_R} + v_c)b_{\beta_R}^\dagger b_{\beta_R}
$$

$$
+ \int d\beta_L\,(\omega_{\beta_L} + v_c)b_{\beta_L}^\dagger b_{\beta_L}, \qquad (A3b)
$$

where left- and right-going modes are labeled by the subscripts L and R. To transfer the Hamiltonian (A2) into real space, we define the Fourier transformations $a_{\alpha_R} = \int dx\, a_R(x)e^{-i\alpha_R x}$, $a_{\alpha_L}^\dagger = \int dx\, a_L^\dagger(x)e^{i\alpha_L x}$, $b_{\beta_R} = \int d\tilde{x}\, b_R(\tilde{x})e^{-i\beta_R\tilde{x}}$, $b_{\beta_R}^\dagger = \int d\tilde{x}\, b_R^\dagger(\tilde{x})e^{i\beta_R\tilde{x}}$, and substituting Eqs. (A3a) and (A3b) into Eq. (A2), we then have

$$
H_{\text{eff}} = \left(\omega_{21} + v_c - \frac{i\gamma_2}{2}\right)|2\rangle\langle2| + \left(\omega_{31} - \frac{i\gamma_3}{2}\right)|3\rangle\langle3| + (\Omega_c|3\rangle\langle2| + \text{H.c.})
$$

$$
- \sum_{l=L,R} f_l \int dx\, a_l^\dagger(x)\left(iv_g\frac{\partial}{\partial x}\right)a_l(x) + \sum_{l=L,R} \int d\tilde{x}\, b_l^\dagger(\tilde{x})\left(v_c - if_l\tilde{v}_g\frac{\partial}{\partial\tilde{x}}\right)b_l(\tilde{x})
$$

$$
+ \tilde{g}_{31}\sum_{l=L,R}\sum_{n=1}^N \int dx\,\delta(x - x_n)(|3\rangle\langle1|a_l(x) + \text{H.c.}) + \tilde{g}_{21}\sum_{l=L,R}\sum_{m=1}^M \int d\tilde{x}\,\delta(\tilde{x} - \tilde{x}_m)(|2\rangle\langle1|b_l(\tilde{x}) + \text{H.c.}), \qquad (A4)
$$

with $\tilde{g}_{3(2)1} = \sqrt{2\pi}g_{3(2)1}$. Note that we additionally introduce $i\gamma_{2(3)}$ to describe the nonwaveguide loss of the atom, which can be obtained by writing down the full system-environment Hamiltonian and eliminating the variables of environments [32].

Substituting Eq. (1) and Eq. (3) into the stationary Schrödinger equation $H_{\text{eff}}|\Psi\rangle = \omega|\Psi\rangle$, one can obtain the following differential equations:

$$
\left(-iv_g\frac{\partial}{\partial x} - \omega\right)\phi_R^\alpha(x) + e_3\tilde{g}_{31}\sum_{n=1}^N \delta(x - x_n) = 0, \quad \left(iv_g\frac{\partial}{\partial x} - \omega\right)\phi_L^\alpha(x) + e_3\tilde{g}_{31}\sum_{n=1}^N \delta(x - x_n) = 0,
$$

$$
\left(-i\tilde{v}_g\frac{\partial}{\partial\tilde{x}} + v_c - \omega\right)\phi_R^\beta(\tilde{x}) + e_2\tilde{g}_{21}\sum_{m=1}^M \delta(\tilde{x} - \tilde{x}_m) = 0, \quad \left(i\tilde{v}_g\frac{\partial}{\partial\tilde{x}} + v_c - \omega\right)\phi_L^\beta(\tilde{x}) + e_2\tilde{g}_{21}\sum_{m=1}^M \delta(\tilde{x} - \tilde{x}_m) = 0,
$$

$$
e_2(\omega_{21} + v_c - \omega) + e_3\Omega_c^* + \tilde{g}_{21}\sum_{m=1}^M \left[\phi_R^\beta(\tilde{x}_m) + \phi_L^\beta(\tilde{x}_m)\right] = 0, \quad e_3(\omega_{31} - \omega) + e_2\Omega_c + \tilde{g}_{31}\sum_{n=1}^N \left[\phi_R^\alpha(x_n) + \phi_L^\alpha(x_n)\right] = 0, \quad (A5)
$$

where $\phi_{R(L)}^{\alpha(\beta)}$ are defined in Eqs. (3a)–(3d). The Dirac δ functions demonstrate that the wave function is discontinuous at the scattering point $x_n(\tilde{x}_m)$. Therefore, we can divide the whole scattering into several intervals, i.e., the scattering for the giant atom can be considered as that for a series of cascaded small atoms. This is the reason for the Fig. 2.

The corresponding solutions of Eq. (A5) can be obtained by taking integrations over the interval $x \in [x_n^-, x_n^+]$, $\tilde{x} \in [\tilde{x}_m^-, \tilde{x}_m^+]$ such that the scattering amplitudes read

$$t_N = \frac{\left(\Delta_{31} - \Delta_{32} - \Delta_r^{(M)} + \frac{i\gamma_2}{2} + i\Gamma_{21}^{(M)}\right)\left(\Delta_{31} - \Delta_L^{(N)} + \frac{i\gamma_3}{2}\right) - |\Omega_c|^2}{\left(\Delta_{31} - \Delta_{32} - \Delta_r^{(M)} + \frac{i\gamma_2}{2} + i\Gamma_{21}^{(M)}\right)\left(\Delta_{31} - \Delta_L^{(N)} + \frac{i\gamma_3}{2} + i\Gamma_{31}^{(N)}\right) - |\Omega_c|^2},$$ (A6a)

$$e_3 = \frac{\left(\Delta_{31} - \Delta_{32} - \Delta_r^{(M)} + \frac{i\gamma_2}{2} + i\Gamma_{21}^{(M)}\right)\tilde{g}_{31} \sum_{n=1}^{N} e^{(N-n)i(\Delta_{31}\tau + \phi)}}{\left(\Delta_{31} - \Delta_{32} - \Delta_r^{(M)} + i\Gamma_{21}^{(M)}\right)\left(\Delta_{31} - \Delta_L^{(N)} + \frac{i\gamma_3}{2} + i\Gamma_{31}^{(N)}\right) - |\Omega_c|^2},$$ (A6b)

$$\tilde{t}_M = -\frac{i\Omega_c^*}{\tilde{v}_g} \frac{\tilde{g}_{21} \sum_{m=1}^{M} e^{-(M-m)i\omega_\beta\tilde{\tau}} \tilde{g}_{31} \sum_{n=1}^{N} e^{(N-n)i(\Delta_{31}\tau + \phi)}}{\left(\Delta_{31} - \Delta_{32} - \Delta_r^{(M)} + i\Gamma_{21}^{(M)}\right)\left(\Delta_{31} - \Delta_L^{(N)} + \frac{i\gamma_3}{2} + i\Gamma_{31}^{(N)}\right) - |\Omega_c|^2},$$ (A6c)

$$\tilde{r}_1 = -\frac{i\Omega_c^*}{\tilde{v}_g} \frac{\tilde{g}_{21} \sum_{m=1}^{M} e^{(M-m)i\omega_\beta\tilde{\tau}} \tilde{g}_{31} \sum_{n=1}^{N} e^{(N-n)i(\Delta_{31}\tau + \phi)}}{\left(\Delta_{31} - \Delta_{32} - \Delta_r^{(M)} + i\Gamma_{21}^{(M)}\right)\left(\Delta_{31} - \Delta_L^{(N)} + \frac{i\gamma_3}{2} + i\Gamma_{31}^{(N)}\right) - |\Omega_c|^2},$$ (A6d)

where $\Delta_r^{(M)}$, $\Gamma_{21}^{(M)}$, $\Delta_L^{(N)}\Gamma_{31}^{(N)}$ are defined in Eqs. (6)–(9). The first two equations are Eqs. (4a) and (4b), and the last two equations denote the scattering in the waveguide B. Notably, if we choose $M = 1, N = 2$ and $\Omega_c = 0$, the transmission amplitude t_N reduces to that of a two-level giant atom [12,16].

According to Eqs. (A6c)–(A6d), one can always find a condition $\sum_{m=1}^{N} \exp[(M - m)i\omega_\beta\tilde{\tau}] = 0$ for a given M such that $\tilde{t}_M = \tilde{r}_1 = 0$, which means that the incident single photon cannot be detected in the waveguide B, i.e., the system does not involve frequency conversions [34,35]. For instance, if we choose $M = 2$ (the case we discussed in the main text), this condition becomes $\omega_\beta\tilde{\tau} = (2k + 1)\pi$, which is also the condition of eliminating the undesired spontaneous transition $|1\rangle \leftrightarrow |2\rangle$.

APPENDIX B: STANDARD EIT IN A SMALL ATOM

According to Eq. (4a), the giant atom reduces to a small atom when $N = 1$. Therefore, the system can exhibit a standard EIT or ATS phenomenon depending on the Rabi frequency Ω_c [32,33], as shown in Fig. 8 with

$$t_1 = \frac{\left(\Delta_{31} - \Delta_{32} + \frac{i\gamma_2}{2}\right)\left(\Delta_{31} + \frac{i\gamma_3}{2}\right) - |\Omega_c|^2}{\left(\Delta_{31} - \Delta_{32} + \frac{i\gamma_2}{2}\right)\left(\Delta_{31} + \frac{i\gamma_3}{2} + \frac{i\Gamma_{31}}{2}\right) - |\Omega_c|^2}. \quad \text{(B1)}$$

As Ω_c increases from zero, the system gradually enters from the resonance absorption to the EIT and then to the ATS regimes, as shown in Fig. 8(a). Both EIT and ATS phenomena can be well explained by *dressed states*. The strong control field Ω_c makes the bare level $|3\rangle$ split into two dressed states $|3^+\rangle$ and $|3^-\rangle$ which are spaced by $2\Omega_c$. Therefore, there exist two excitation pathways for the transition $|1\rangle \rightarrow |3\rangle$ pumped by the probe field Ω_p: (1) $|1\rangle \rightarrow |3^+\rangle \rightarrow |3\rangle$ pathway and (2) $|1\rangle \rightarrow |3^-\rangle \rightarrow |3\rangle$ pathway. These two pathways have equal but opposite probability amplitudes. In the EIT regime, destructive interference occurs between two pathways, making the atom transparent for the probe field [24–26]. Thereby, the spectrum exhibits a sharp transparent peak at two-photon resonance $\Delta_{31} = \Delta_{32}$, shown as the red dashed line in Fig. 8(a) and Fig. 8(b). However, destructive interference does not occur in the ATS regime [40]. Hence the spectrum exhibits two absorption peaks corresponding to the dressed states at the single-photon resonances $\Delta_{31} = \pm\Omega_c$, shown as the black

dotted line in Fig. 8(a). Figures 8(c) and 8(d) show the influences of nonwaveguide loss γ_2 and γ_3 in the EIT regime. As the loss γ_2 increases, the transparency peak gradually decreases until disappears, as shown in Fig. 8(c). This is because the increasing γ_2 breaks the strong field condition $\Omega_c \gg \sqrt{\Gamma_{31}\gamma_2}/2$, which is necessary for EIT. In addition, the increase of loss γ_3 induces a decrease in absorption, as shown in Fig. 8(d). This is because the loss γ_3 presents in the term of single-photon resonance, and thus it represents the loss of the absorption. The above discussions also apply to giant atoms; we do not provide it in the main text for brevity.
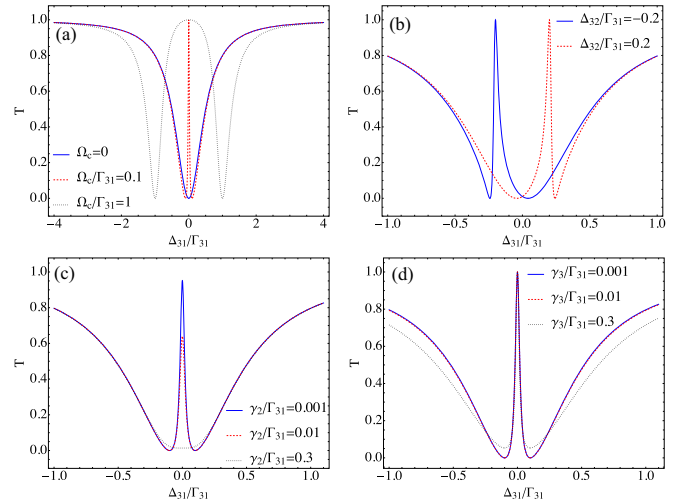

FIG. 8. Transmission spectra for a small atom ($N = 1$). Parameters used in plotting are in (a) $\Delta_{32} = \gamma_2 = \gamma_3 = 0$, in (b) $\Omega_c = 0.1\Gamma_{31}$ and $\gamma_2 = \gamma_3 = 0$, in (c) $\Omega_c = 0.1\Gamma_{31}$ and $\Delta_{32} = \gamma_3 = 0$, and in (d) $\Omega_c = 0.1\Gamma_{31}$ and $\Delta_{32} = \gamma_2 = 0$. (a) As Rabi frequency Ω_c increases, the system gradually enters the resonance absorption regime (blue solid line), EIT regime (red dashed line), and ATS regime (black dotted line). (b) The influence of the detuing Δ_{32}. Since the induced transparency occurs at two-photon resonance, the transparency peak is shifted by the detuning Δ_{32}. (c) The influence of the loss γ_2. As the loss γ_2 increases, the transparency peak gradually decreases until disappear. This is because a large loss γ_2 breaks the strong field condition $\Omega_c \gg \sqrt{\Gamma_{31}\gamma_2}/2$. (d) The influence of the loss γ_3. The efficiency of absorption decreases as the loss γ_3 increases.

APPENDIX C: DERIVATION OF MASTER EQUATIONS

In contrast to the original Hamiltonian (A1), we consider a classical input Ω_p with position-dependent phase $\exp(i\alpha x_n)$ describing the propagation effects enters the atom from the waveguide A, such that the Hamiltonian of a Δ-type giant atom is then given by

$$
\begin{aligned}
H_\Delta = {} & \sum_{i=1}^{3} \omega_i |i\rangle\langle i| + \sum_{n=1}^{N} (\Omega_p e^{-i\omega t + i\alpha x_n} |3\rangle\langle 1| + \text{H.c.}) \\
& + (\Omega_c e^{-iv_c t} |3\rangle\langle 2| + \text{H.c.}) \\
& + \int d\alpha\, \omega_\alpha a_\alpha^\dagger a_\alpha + \int d\beta\, \omega_\beta b_\beta^\dagger b_\beta \\
& + \sum_{n=1}^{N} \int d\alpha [g_{31}|3\rangle\langle 1| a_\alpha e^{i\alpha x_n} + \text{H.c.}] \\
& + \sum_{m=1}^{M} \int d\beta [g_{21}|2\rangle\langle 1| b_\beta e^{i\beta \tilde{x}_m} + \text{H.c.}],
\end{aligned} \tag{C1}
$$

where the frequencies of level $|i\rangle$ is ω_i. Thus the interaction Hamiltonian in the interaction picture takes the form

$$
V(t) = V^c(t) + V^q(t),
$$

where $V^c(t)$ is defined in Eq. (12) and

$$
\begin{aligned}
V^q(t) = {} & g_{31} \sum_{n=1}^{N} \int d\alpha \, (|3\rangle\langle 1| a_\alpha e^{-i\Delta_\alpha t + i\alpha x_n} + \text{H.c.}) \\
& + g_{21} \sum_{m=1}^{M} \int d\alpha \, (|2\rangle\langle 1| b_\beta e^{-i\Delta_\beta t + i\beta \tilde{x}_m} + \text{H.c.})
\end{aligned}
$$

with detunings $\Delta_\alpha = \omega_\alpha - \omega_{31} = \omega_\alpha - (\omega_3 - \omega_1)$ and $\Delta_\beta = \omega_\beta - \omega_{21} = \omega_\beta - (\omega_2 - \omega_1)$. Here we also assume $\omega_1 = 0$ as the reference.

The dynamics of the giant atom is governed by the following Born master equation:

$$
\begin{aligned}
\dot{\rho}_a(t) = {} & -i[V^c(t), \rho_a(t)] - i\text{tr}_w[V^q(t), \rho_a(0) \otimes \rho_w(0)] \\
& - \text{tr}_w \int_0^t dt' \, [V^q(t), [V^q(t'), \rho_a(t') \otimes \rho_w(0)]] \\
& + \mathcal{L}_{\text{Loc}}^{n-w} \rho_a(t),
\end{aligned} \tag{C2}
$$

where $\rho_a(t)$ is the atomic density operator in a generic form and $\rho_w(0)$ is the density operator of two waveguides in the initial states. The superoperator $\mathcal{L}_{\text{Loc}}^{n-w} \rho_a(t) = \gamma_{31}\mathcal{D}[|1\rangle\langle 3|]\rho_a(t) + \gamma_{32}\mathcal{D}[|2\rangle\langle 3|]\rho_a(t) + \gamma_2^\phi \mathcal{D}[|2\rangle\langle 2|]\rho_a(t) + \gamma_3^\phi \mathcal{D}[|3\rangle\langle 3|]\rho_a(t)$ denotes evolution governed by the loss to the nonwaveguide degrees of freedom. Notably, the terms related to $V^q(t)$ have been neglected in Sec. VI A.

After taking traces over the variables of waveguides, Eq. (C2) reduces to Eq. (11). Notably, if we perform a Markovian approximation $\rho_a(t') \to \rho_a(t)$, Eq. (C2) reduces to Eq. (19). One can examine that this replacement is equivalent to $\rho_a^q(t - n\tau) \to \rho_a^q(t)$ and $\rho_a^q(t - m\tilde{\tau}) \to \rho_a^q(t)$ in Sec. VI B.

[1] X. Gu, A. F. Kockum, A. Miranowicz, Y.-X. Liu, and F. Nori, Microwave photonics with superconducting quantum circuits, Phys. Rep. **718–719**, 1 (2017).

[2] A. Blais, A. L. Grimsmo, S. M. Girvin, and A. Wallraff, Circuit quantum electrodynamics, Rev. Mod. Phys. **93**, 025005 (2021).

[3] I.-C. Hoi, C. M. Wilson, G. Johansson, T. Palomaki, B. Peropadre, and P. Delsing, Demonstration of a Single-Photon Router in the Microwave Regime, Phys. Rev. Lett. **107**, 073601 (2011).

[4] F. Arute, K. Arya, R. Babbush, D. Bacon, J. C. Bardin, R. Barends, R. Biswas, S. Boixo, F. G. S. L. Brandao, D. A. Buell, B. Burkett, Y. Chen, Z. Chen, B. Chiaro, R. Collins, W. Courtney, A. Dunsworth, E. Farhi, B. Foxen, A. Fowler *et al.*, Quantum supremacy using a programmable superconducting processor, Nature (London) **574**, 505 (2019).

[5] A. Frisk Kockum, P. Delsing, and G. Johansson, Designing frequency-dependent relaxation rates and Lamb shifts for a giant artificial atom, Phys. Rev. A **90**, 013837 (2014).

[6] A. F. Kockum, Quantum optics with giant atoms—The first five years, in *Mathematics for Industry* edited by T. Takagi, M. Wakayama, K. Tanaka, N. Kunihiro, K. Kimoto, and Y. Ikematsu (Springer, Singapore, 2020), pp. 125–146.

[7] M. V. Gustafsson, T. Aref, A. F. Kockum, M. K. Ekström, G. Johansson, and P. Delsing, Propagating phonons coupled to an artificial atom, Science **346**, 207 (2014).

[8] A. F. Kockum, G. Johansson, and F. Nori, Decoherence-Free Interaction between Giant Atoms in Waveguide Quantum Electrodynamics, Phys. Rev. Lett. **120**, 140404 (2018).

[9] M. J. A. Schuetz, E. M. Kessler, G. Giedke, L. M. K. Vandersypen, M. D. Lukin, and J. I. Cirac, Universal Quantum Transducers Based on Surface Acoustic Waves, Phys. Rev. X **5**, 031031 (2015).

[10] Y. Chu, P. Kharel, W. H. Renninger, L. D. Burkhart, L. Frunzio, P. T. Rakich, and R. J. Schoelkopf, Quantum acoustics with superconducting qubits, Science **358**, 199 (2017).

[11] R. Manenti, A. F. Kockum, A. Patterson, T. Behrle, J. Rahamim, G. Tancredi, F. Nori, and P. J. Leek, Circuit quantum acoustodynamics with surface acoustic waves, Nat. Commun. **8**, 975 (2017).

[12] L. Guo, A. Grimsmo, A. F. Kockum, M. Pletyukhov, and G. Johansson, Giant acoustic atom: A single quantum system with a deterministic time delay, Phys. Rev. A **95**, 053821 (2017).

[13] Y. Chu, P. Kharel, T. Yoon, L. Frunzio, P. T. Rakich, and R. J. Schoelkopf, Creation and control of multi-phonon Fock states in a bulk acoustic-wave resonator, Nature (London) **563**, 666 (2018).

[14] K. J. Satzinger, Y. P. Zhong, H.-S. Chang, G. A. Peairs, A. Bienfait, M.-H. Chou, A. Y. Cleland, C. R. Conner, E. Dumur, J. Grebel, I. Gutierrez, B. H. November, R. G. Povey, S. J.

Whiteley, D. D. Awschalom, D. I. Schuster, and A. N. Cleland, Quantum control of surface acoustic-wave phonons, Nature (London) **563**, 661 (2018).

[15] M. K. Ekström, T. Aref, A. Ask, G. Andersson, B. Suri, H. Sanada, G. Johansson, and P. Delsing, Towards phonon routing: Controlling propagating acoustic waves in the quantum regime, New J. Phys. **21**, 123013 (2019).

[16] G. Andersson, B. Suri, L. Guo, T. Aref, and P. Delsing, Non-exponential decay of a giant artificial atom, Nat. Phys. **15**, 1123 (2019).

[17] L. Guo, A. F. Kockum, F. Marquardt, and G. Johansson, Oscillating bound states for a giant atom, Phys. Rev. Res. **2**, 043014 (2020).

[18] B. Kannan, M. J. Ruckriegel, D. L. Campbell, A. Frisk Kockum, J. Braumuller, D. K. Kim, M. Kjaergaard, P. Krantz, A. Melville, B. M. Niedzielski, A. Vepsalainen, R. Winik, J. L. Yoder, F. Nori, T. P. Orlando, S. Gustavsson, and W. D. Oliver, Waveguide quantum electrodynamics with superconducting artificial giant atoms, Nature (London) **583**, 775 (2020).

[19] L. Du and Y. Li, Single-photon frequency conversion via a giant Λ-type atom, Phys. Rev. A **104**, 023712 (2021).

[20] L. Du, M.-R. Cai, J.-H. Wu, Z. Wang, and Y. Li, Single-photon nonreciprocal excitation transfer with non-Markovian retarded effects, Phys. Rev. A **103**, 053701 (2021).

[21] Q. Y. Cai and W. Z. Jia, Coherent single-photon scattering spectra for a giant-atom waveguide-QED system beyond the dipole approximation, Phys. Rev. A **104**, 033710 (2021).

[22] S. L. Feng and W. Z. Jia, Manipulating single-photon transport in a waveguide-QED structure containing two giant atoms, Phys. Rev. A **104**, 063712 (2021).

[23] P. Delsing, A. N. Cleland, M. J. A. Schuetz, J. Knörzer, G. Giedke, J. I. Cirac, K. Srinivasan, M. Wu, K. C. Balram, C. Bäuerle, T. Meunier, C. J. Ford, P. V. Santos, E. Cerda-Méndez, H. Wang, H. J. Krenner, E. D. S. Nysten, M. Weiß, G. R. Nash, L. Thevenard *et al.*, The 2019 surface acoustic waves roadmap, J. Phys. D **52**, 353001 (2019).

[24] S. E. Harris, J. E. Field, and A. Imamoglu, Nonlinear Optical Processes using Electromagnetically Induced Transparency, Phys. Rev. Lett. **64**, 1107 (1990).

[25] K.-J. Boller, A. Imamoglu, and S. E. Harris, Observation of Electromagnetically Induced Transparency, Phys. Rev. Lett. **66**, 2593 (1991).

[26] M. Fleischhauer, A. Imamoglu, and J. P. Marangos, Electromagnetically induced transparency: Optics in coherent media, Rev. Mod. Phys. **77**, 633 (2005).

[27] A. A. Abdumalikov, O. Astafiev, A. M. Zagoskin, Y. A. Pashkin, Y. Nakamura, and J. S. Tsai, Electromagnetically Induced Transparency on a Single Artificial Atom, Phys. Rev. Lett. **104**, 193601 (2010).

[28] Y.-L. L. Fang and H. U. Baranger, Multiple emitters in a waveguide: Nonreciprocity and correlated photons at perfect elastic transmission, Phys. Rev. A **96**, 013842 (2017).

[29] D. Mukhopadhyay and G. S. Agarwal, Transparency in a chain of disparate quantum emitters strongly coupled to a waveguide, Phys. Rev. A **101**, 063814 (2020).

[30] G. Andersson, M. K. Ekström, and P. Delsing, Electromagnetically Induced Acoustic Transparency with a Superconducting Circuit, Phys. Rev. Lett. **124**, 240402 (2020).

[31] A. M. Vadiraj, A. Ask, T. G. McConkey, I. Nsanzineza, C. W. S. Chang, A. F. Kockum, and C. M. Wilson, Engineering the level structure of a giant artificial atom in waveguide quantum electrodynamics, Phys. Rev. A **103**, 023710 (2021).

[32] J.-T. Shen and S. Fan, Theory of single-photon transport in a single-mode waveguide. I. Coupling to a cavity containing a two-level atom, Phys. Rev. A **79**, 023837 (2009).

[33] Y. T. Zhu and W. Z. Jia, Single-photon quantum router in the microwave regime utilizing double superconducting resonators with tunable coupling, Phys. Rev. A **99**, 063815 (2019).

[34] W. Z. Jia, Y. W. Wang, and Y.-X. Liu, Efficient single-photon frequency conversion in the microwave domain using superconducting quantum circuits, Phys. Rev. A **96**, 053832 (2017).

[35] M. Bradford and J.-T. Shen, Single-photon frequency conversion by exploiting quantum interference, Phys. Rev. A **85**, 043814 (2012).

[36] J. Gough and M. R. James, The series product and its application to quantum feedforward and feedback networks, IEEE Trans. Autom. Control **54**, 2530 (2009).

[37] V. E. Manucharyan, J. Koch, L. I. Glazman, and M. H. Devoret, Fluxonium: Single cooper-pair circuit free of charge offsets, Science **326**, 113 (2009).

[38] S. Novikov, T. Sweeney, J. E. Robinson, S. P. Premaratne, B. Suri, F. C. Wellstood, and B. S. Palmer, Raman coherence in a circuit quantum electrodynamics Lambda system, Nat. Phys. **12**, 75 (2016).

[39] J. Long, H. S. Ku, X. Wu, X. Gu, R. E. Lake, M. Bal, Y.-X. Liu, and D. P. Pappas, Electromagnetically Induced Transparency in Circuit Quantum Electrodynamics with Nested Polariton States, Phys. Rev. Lett. **120**, 083602 (2018).

[40] S. H. Autler and C. H. Townes, Stark effect in rapidly varying fields, Phys. Rev. **100**, 703 (1955).

[41] M. Baur, S. Filipp, R. Bianchetti, J. M. Fink, M. Göppl, L. Steffen, P. J. Leek, A. Blais, and A. Wallraff, Measurement of Autler-Townes and Mollow Transitions in a Strongly Driven Superconducting Qubit, Phys. Rev. Lett. **102**, 243602 (2009).

[42] M. A. Sillanpää, J. Li, K. Cicak, F. Altomare, J. I. Park, R. W. Simmonds, G. S. Paraoanu, and P. J. Hakonen, Autler-Townes Effect in a Superconducting Three-Level System, Phys. Rev. Lett. **103**, 193601 (2009).

[43] S. Novikov, J. E. Robinson, Z. K. Keane, B. Suri, F. C. Wellstood, and B. S. Palmer, Autler-Townes splitting in a three-dimensional transmon superconducting qubit, Phys. Rev. B **88**, 060503(R) (2013).

[44] J. Li, G. S. Paraoanu, K. Cicak, F. Altomare, J. I. Park, R. W. Simmonds, M. A. Sillanpää, and P. J. Hakonen, Dynamical Autler-Townes control of a phase qubit, Sci. Rep. **2**, 645 (2012).

[45] N. Német, A. Carmele, S. Parkins, and A. Knorr, Comparison between continuous- and discrete-mode coherent feedback for the Jaynes-Cummings model, Phys. Rev. A **100**, 023805 (2019).

[46] M. O. Scully and M. S. Zubairy, in *Quantum Optics* (Cambridge University Press, New York, 1997), pp. 225–229.

[47] H.-P. Breuer, E.-M. Laine, J. Piilo, and B. Vacchini, Colloquium: Non-Markovian dynamics in open quantum systems, Rev. Mod. Phys. **88**, 021002 (2016).

[48] S.-B. Xue, R.-B. Wu, W.-M. Zhang, J. Zhang, C.-W. Li, and T.-J. Tarn, Decoherence suppression via non-Markovian coherent feedback control, Phys. Rev. A **86**, 052304 (2012).

[49] W.-M. Zhang, P.-Y. Lo, H.-N. Xiong, M. W.-Y. Tu, and F. Nori, General Non-Markovian Dynamics of Open Quantum Systems, Phys. Rev. Lett. **109**, 170402 (2012).

[50] S. Weis, R. Rivière, S. Deléglise, E. Gavartin, O. Arcizet, A. Schliesser, and T. J. Kippenberg, Optomechanically induced transparency, Science **330**, 1520 (2010).

[51] W. Z. Jia, L. F. Wei, Y. Li, and Y.-x. Liu, Phase-dependent optical response properties in an optomechanical system by coherently driving the mechanical resonator, Phys. Rev. A **91**, 043843 (2015).

[52] H.-K. Lau and A. A. Clerk, Fundamental limits and non-reciprocal approaches in non-Hermitian quantum sensing, Nat. Commun. **9**, 4320 (2018).

[53] Y. T. Zhu, R. B. Wu, Z. H. Peng, and S. Xue, Giant-cavity-based quantum sensors with enhanced performance, Front. Phys. **10**, 896596 (2022).

[54] Y.-L. L. Fang and H. U. Baranger, Waveguide QED: Power spectra and correlations of two photons scattered off multiple distant qubits and a mirror, Phys. Rev. A **91**, 053845 (2015).

[55] G. Calajó, Y.-L. L. Fang, H. U. Baranger, and F. Ciccarello, Exciting a Bound State in the Continuum through Multiphoton Scattering Plus Delayed Quantum Feedback, Phys. Rev. Lett. **122**, 073601 (2019).

[56] S. Xue, R. Wu, M. R. Hush, and T.-J. Tarn, Non-Markovian coherent feedback control of quantum dot systems, Quantum Sci. Technol. **2**, 014002 (2017).

[57] S. Xue, M. R. Hush, and I. R. Petersen, Feedback tracking control of non-Markovian quantum systems, IEEE Trans. Contr. Syst. Technol. **25**, 1552 (2017).

[58] S. Xue, T. Nguyen, M. R. James, A. Shabani, V. Ugrinovskii, and I. R. Petersen, Modeling for non-Markovian quantum systems, IEEE Trans. Contr. Syst. Technol. **28**, 2564 (2020).

[59] M. Afzelius, N. Gisin, and H. Riedmatten, Quantum memory for photons, Phys. Today **68**, 42 (2015).

[60] A. Kasapi, M. Jain, G. Y. Yin, and S. E. Harris, Electromagnetically Induced Transparency: Propagation Dynamics, Phys. Rev. Lett. **74**, 2447 (1995).

[61] M. Xiao, Y.-Q. Li, S.-Z. Jin, and J. Gea-Banacloche, Measurement of Dispersive Properties of Electromagnetically Induced Transparency in Rubidium Atoms, Phys. Rev. Lett. **74**, 666 (1995).

[62] H. Schmidt and A. Imamoglu, Giant Kerr nonlinearities obtained by electromagnetically induced transparency, Opt. Lett. **21**, 1936 (1996).

[63] M. O. Scully, S.-Y. Zhu, and A. Gavrielides, Degenerate Quantum-Beat Laser: Lasing without Inversion and Inversion without Lasing, Phys. Rev. Lett. **62**, 2813 (1989).

[64] E. S. Fry, X. Li, D. Nikonov, G. G. Padmabandu, M. O. Scully, A. V. Smith, F. K. Tittel, C. Wang, S. R. Wilkinson, and S.-Y. Zhu, Atomic Coherence Effects within the Sodium d_1 Line: Lasing without Inversion via Population Trapping, Phys. Rev. Lett. **70**, 3235 (1993).

[65] A. Nottelmann, C. Peters, and W. Lange, Inversionless Amplification of Picosecond Pulses Due to Zeeman Coherence, Phys. Rev. Lett. **70**, 1783 (1993).